Modeling of the impact of the soil roughness on PolSAR images

Flora Weissgerber, Elise Colin-Koeniguer, Nicolas Trouvé

Modeling of the impact of the soil roughness on PolSAR images

Flora Weissgerber[a], Elise Colin-Koeniguer[a], and Nicolas Trouvé[a]
[a]ONERA, Université Paris Saclay, F-91123 Palaiseau - France

Abstract

The PolSAR response of a surface depends of multiple parameters, amongst which the variation of radar backscatter with the incidence angle and its roughness. To investigate the coupling between these parameters, we model the terrain as a layer of scatterers, defined by their position, their normal and a complex RCS. The SAR image is computed from the coherent sum of the scatterers directly in the SAR geometry. We show that a difference in backscattered energy between the polarimetric channel can be rendered by this simple modeling, and that some terrains lead to a decorrelation between the polarimetric channels.

1 Introduction

Polarimetric applications are based on the assumption that different type of scatterers lead to different polarimetric backscattering. This is especially true for polarimetric classification for which the physical modelling impact the definition of classes as well as the developed algorithm.

The differences in behaviour is often stressed between surfaces and volumetric scattering [1] but surface roughness has also an impact on the radar backscatter [2], on the ratio between the polarimetric backscatter [2, 3] and on the degree of coherence between the polarimetric channel [4, 5]. This impact is underlined for smooth surfaces when the rms of the height variation of the surface in the order of magnitude of the wavelength.

Textural information appears in SAR images, highlighting the impact of the spatial distribution of the variation of height as the scales of multiple pixels and thus a scale way coarser than the wavelength.

When working in X-band or higher, having the knowledge of the surface height variation at the scale of the wavelength would require a special ground campaign. In this article, we investigate the possibility of reproducing the macro behaviour, i.e. the one that can be measured on a SAR image, with a level of details on the ground description in the order of magnitude of 10 times the wavelength. This level of description is in itself not often available but can be constructed from remote sensed optical images that have a resolution below one meter. Different types of surfaces having the same height standard deviation are compared to assess the influence of the spatial distribution of the variation of height.

The scattering model used in this work is presented in section 2 while the simulation process that enables to test the model is describes in section 3. The experimental data sets are described in section 5.1. The impact of the surface roughness and the electromagnetic properties on the retrieval of the radar backscatter, and the obtained degree of coherence is discussed in section 4 in the case of a random terrain and in section 5 for terrains derived from scanned materials. Conclusive remarks are given in section 6.

2 Modeling of the SAR acquisition

The interaction between the incident electromagnetic field emitted by the radar and the terrain is computed using a simple Kirchhoff approximation where the surface are locally approximated by a plane which electromagnetic response is summarized in a single scatterer. The continuous surface is thus represented by a collection of scatterers, which backscattering can be modeled as radiating antennas.

The position P of the scatterers are deduced from the geometry of the surface, while there electromagnetic response is summarized in the scatterer radiating diagram. Making the hypothesis that the only parameter influencing the backscattering is the local incidence angle θ_s, the radiating power of each scatterers is deduced from the Radar Cross Section (RCS) curve (also called σ_0-curve), that depends of the scatterer material and of the polarimetric channel. The σ_0-curves for the two materials used in this article, extracted from [6], is presented in Figure 1. The surface of all the scatterer is supposed to be equal to 1m^2 independently of the grid on which they are positioned. The σ_0 value is thus used as the power value and converted to energy to assign the modulus of each scatterer. This local incidence angle is determined using the normal $\mathbf{n}$ to plane from the kirchhoff approximation.

In this first version, the power reduction of the incidence field due to the variation of the distance r_s between the emitting antenna and the scatterers is not taken into account. The propagation of the electromagnetic field is only taken into account by the phase of the field radiated by the scatterers and measured at the radar antenna. It is computed from the optical path between the radar antenna and the scatterers, in a mono-static configuration (the emitting radar antenna is the same than the receiving radar antenna) : $\varphi_P = \frac{4\pi}{\lambda} r_s$.

Using to the position of the scatterers, their phase φ_0 can be modulated by the phase due to the optical path

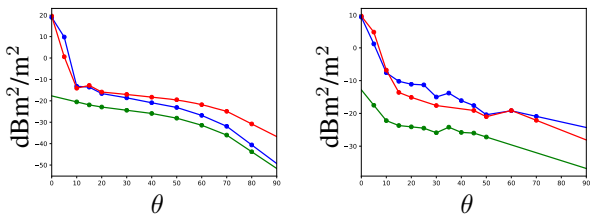

(a) (b)

Figure 1 σ_0 curves of (a) Asphalt in X-band and (b) Forage Crop in L-band. – HH, – HV, – VV. The measurement is represented by a bullet while the interpolation is represented by a line.

φ_P. The complex RCS $re^{i\varphi}$ of each scatterer is thus $10^{\frac{\sigma_0(\theta_s)}{20}} e^{i(\varphi_0+\varphi_P)}$, with the scatterer initial phase φ_0 common for the four polarimetric channels.

The SAR image construction is based on the hypothesis that the electromagnetic field emitted by all scatterers in a resolution cell will be coherently summed at the radar antenna. The SAR images formation model is thus close to the hypothesis made by Goodman [7] to model the fully-developped speckle phenomenon : the complexe RCS of a large number of scatterers present in the same resolution cell is coherently summed during the acquisition. Goodman made the hypothesis that enough scatterers where in the resolution cell to use the central-limit theorem. In [8], we have shown that the number of scatterers could be quite small (above 10) in order to retreave the fully-developped speckle statistics, even with constant RCS absolute value. In that case, more than 50 scatterers are needed to retrieve the extreme values of speckle [9]. The modulus of the SAR image pixel follows a Rayleigh distribution of parameter μ: $\rho \sim \mathcal{R}(\mu) = \frac{2}{\mu}\frac{\rho}{\mu} e^{-\left(\frac{\rho}{\mu}\right)^2}$ and the SAR image pixel phase ϕ follows a uniform distribution on a 2π-interval. If all the scatterers are iid and their phase equi-distributed on a 2π-interval, the parameter of the Rayleigh distribution can be deduced from the second moment of r, the scatterers modulus distribution : $\mu = \sqrt{\mathbb{E}(r^2)}$

The resolution cell of the SAR sensor can be deduced from its 2D-PSF represented in Figure 2. It results from two different process in the azimut and range direction. In slant-range, the matching filter of the emitted chirp leads to a sinc PSF. In azimut, the synthesis of the raw data leads to a sinc PSF.

The main points of the model are the following :

- The terrain is represented as a collection of emitting antenna which contribution depends on their local incidence angle, through a σ_0-curve that depends on the polarimetric channel.
- The interaction between the scatterers are represented by a coherent summation of the EM-field emitted by the scatterers in the same SAR resolution cell at the radar antenna.
- The phase of this EM-field is given by the back and forth propagation of the wave emitted by the sensor along the optical path between the radar antenna and the scatterer $\varphi_P = \frac{4\pi}{\lambda} r_s$ where r_s is the distance between the scatterers and the radar antenna. The phase is the same for the four polarimetric channels.

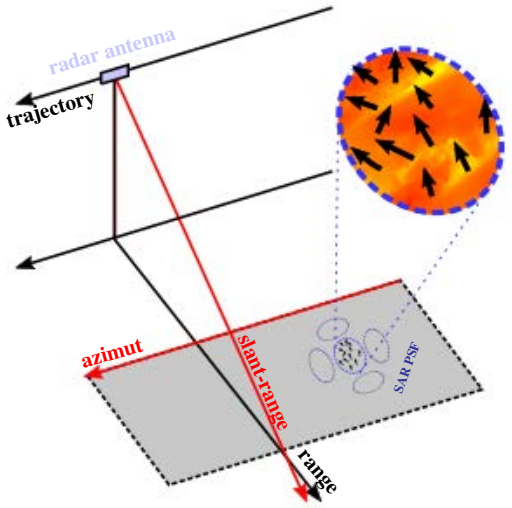

Figure 2 Schematic view of our SAR acquisition model. The 2D-sinc PSD of the SAR sensor is represented in blue dotted line. The black arrows represent the normal of the designated scatterers.

3 Constructing a SAR image

As mentioned in the previous section, the SAR image formation required two steps : the range detection, that leads to the (slant-)range resolution cell and the synthesis, that leads to the azimut resolution cell. In our simulation workflow, the two steps of range detection and synthetis are merged and the complex summation is done directly in the azimut-slant range grid. However, it is still important to apply the SAR PSF to recreate a meaningful image. The complex summation is thus done in an oversampled grid. The final image is obtained by spectral downsampling, adding zero-padding margins. This downsampling is equivalent to apply a cardinal-sine function to all the scatterers.

The main steps of the algorithm are the following :

1. Computation of the position of each scatterers in the azimut-slant range grid (a, r_s)
2. Computation of the RCS of each scatterers
3. Coherent summation of the scatterers RCS in an oversampled grid
4. Downsampling of the image to obtain the final SAR image.

3.1 Computation of the position of the scatterers in the azimut-slant range grid.

Both the terrain and the sensor displacement are described in Cartesian coordinate. The acquisition is supposed to

be done stripmap mode, the sensor moving in an iso-altitude uniform linear motion defined by a speed vector $\mathbf{v} = (v_x, v_y, 0)$ and an initial point in the trajectory computed from the incidence angle θ and the sensor height H specified by the user.
First, the azimut a of each scatterers is computed. It corresponds to the position of the sensor in the centre of their synthetic antenna. We are considering only non-squinted acquisition, a can then be computed from the scalar product between the vector defining the trajectory $\mathbf{t} = \frac{\mathbf{v}}{||\mathbf{v}||}$ and $P = (x, y, z)$. From a, the Cartesian coordinate corresponding to position of the sensor at the centre of the synthetic antenna P_s are then computed for each scatterer. Knowing P_s and P allows to compute the slant range r_s.

3.2 Computation of the RCS.

The radar backscatter r of each scatterer is obtained from the local incidence angle θ_s through a σ_0-curve that depends on the material. The σ_0-curve for the material presented in this article can be observed in figure 1.
For each scatterer, θ_s is computed from the position of the sensor at the center of the synthetic antenna P_s and the normal associated which is scatterers.
For the experiments in this article, the initial phase φ_0 of the scatterers is a constant phase of 0 for all the scatterers. Their phase variation is due the propagation phase $\varphi_P = \frac{4\pi}{\lambda} r_s$.

3.3 Coherent Summation

Each pixel of the SAR image $\mathrm{p} = \rho e^{i\phi}$ is obtained through the complex summation of the N_s scatterers present in the resolution cell :

$$\mathrm{p} = \rho e^{i\phi} = \frac{1}{\sqrt{N_s}} \sum_{n=1}^{N_s} r_n e^{i\varphi_n} \tag{1}$$

The normalisation coefficient $\frac{1}{\sqrt{N_s}}$ enables to get a finite second moment of the speckle distribution. It is used to compensate the fact that multiple resolution cells will have a different number of scatterers and still following the same distribution. However, this statistical choice doesn't reproduce effects such as contraction due to slope if it is not included in the σ_0 curve.
The selection of the scatterers in the resolution cell is done using an image resolution in azimut δ_a and slant range δ_{r_s} set by the user and the oversampling factor in azimut $f_{grid,a}$ and in slant range $f_{grid,sr}$.

3.4 Downsampling

The downsampling is done spectrally. The frequencies corresponding to the non-oversampled grid a selected knowing the oversampling factors in azimut $f_{grid,a}$ and in slant range $f_{grid,sr}$. The final image is obtained by spectral downsampling, adding zero-padding margins directed by the parameters $f_{image,a}$ and $f_{image,sr}$.
This downsampling allows to apply a cardinal-sine to the oversampled pixels. The goal is thus to have as few scatterers as possible summed in the oversampled grid, ideally only one by resolution cell. Moreover, the cardinal-sine is apply as if the scatterer was in the middle of the oversampled resolution cell. Increasing the oversampling factor enables to reproduce more finely the interaction between the scatterers and their neighbours. However, the oversampling factor has a great impact on the processing time and a trade-off has to be defined.

3.5 Measuring the incidence angle by resolution cell

To assess the retrieval of the macro-parameter, it is important to measure the angle of incidence in each resolution cell. To do so, we use the SAR-image-formation process using scatterers with a constant modulus and the phase equal to the local incidence angle in radian :

$$Re^{i\theta_m} = \frac{1}{N_s} \sum_{n=1}^{N_s} e^{i\theta_{s\,n}} \tag{2}$$

where θ_m represents the mean incidence angle. The parameter R can be linked to the mean resultant length [10], indicating if the distribution of θ_s is concentrated around θ_m, when R is close to 1, or more spread, when R is close to 0. Due to the undersampling and zero-padding processes, the value of R can be superior to 1.

4 Results on random terrains

In order to get mathematical keys to analyze the result on the selected terrains, we start by analyzing the impact of the σ_0-curve and the scatterers' phase on the response of random terrain. To do so, two parameters will be studied :

- The modulus distribution
- The degree of coherence

4.1 Model

The electromagnetic influence of the terrain is done, in the presented model, through the local incidence angle, that influence the power backscatter by the scatterers, and through the propagation phase. The scatterers position is supposed to sample uniformly the phase of the electromagnetic field. The propagation phase is thus modeled as an uniform distribution on a 2π-interval. To study the influence of the local incidence angle θ_s distribution on the retrieval of the polarimetric parameters, the local incidence angle is set to follow a normal distribution $\theta_s \sim \mathcal{N}(m_{\theta_s}, s_{\theta_s})$.
Since the local incidence angle is included in the [0, 90] interval, the normal distribution is truncated when m_{θ_s} is close to the boundary of θ_s or when s_{θ_s} is large. As we linearly interpolate the measurement in to compute the σ_0-curve, we approximate it as linear $\sigma_0(\theta_s) = \mathrm{a_{dB}}(\theta_s - m_{\theta_s}) + \mathrm{b_{dB}}$ in this statistical analysis.
With these models, the distribution of the variable $\sigma_0(\theta_s)$ is also a normal distribution, with the following parameters : $\sigma_0 \sim \mathcal{N}(\mathrm{b_{dB}}, \mathrm{a_{dB}} s_{\theta_s})$. Going from dB to amplitude distribution is equivalent to taking the exponential of

$\frac{\ln(10)}{20}\sigma_0$. From which the distribution of the scatterers' modulus r can be obtained as a log-normal distribution $r \sim \mathcal{L}(m_r, s_r) = \frac{1}{r\sqrt{2\pi}s_r} e^{-\frac{(\ln r - m_r)^2}{2s_r^2}}$ with $m_r = \frac{\ln(10)}{20}\mathrm{b_{dB}}$ and $s_r = \frac{\ln(10)}{20}\mathrm{a_{dB}}s_{\theta_s}$.

4.2 The modulus distribution

Knowing the expression of the second moment of the log-normal distribution, the parameter of the Rayleigh distribution of the pixel modulus ρ, μ, can be computed :

$$\mu = \sqrt{e^{2m_r + 2s_r^2}} = e^{\frac{\ln(10)}{20}\mathrm{b_{dB}} + (\frac{\ln(10)}{20}\mathrm{a_{dB}}s_{\theta_s})^2}$$

This equation shows that we don't retrieve the input σ_0-curve as an output of the simulation if the incidence angle distribution has a variance. The difference between the input and the output σ_0-curve increases with both the variance of the θ distribution and the square of the σ_0-curve's slope.

However, the ratio of the parameters from two polarimetric channels p and q has the following equation :

$$\frac{\mu_\mathrm{p}}{\mu_\mathrm{q}} = e^{\frac{\ln(10)}{20}(\mathrm{b_{dBp}} - \mathrm{b_{dBq}}) + (\frac{\ln(10)}{20}(\mathrm{a_{dBp}}^2 - \mathrm{a_{dBq}}^2)s_{\theta_s}^2)}$$

which shows that the ratio between the output σ_0-curves in two polarizations will be retrieve if the two input curves have the same slope square.

4.3 The degree of coherence

The degree of coherence, $\gamma_{\mathrm{p,q}}$ is also a way to compare two polarimetric channels p and q. Given $\mathrm{p_p} = \rho_\mathrm{p} e^{i\phi_\mathrm{p}}$ and $\mathrm{p_q} = \rho_\mathrm{q} e^{-i\phi_\mathrm{q}}$, the pixels in the two polarimetric channels, $\gamma_{\mathrm{p,q}}$ can be written as :

$$\gamma_{\mathrm{p,q}} = \frac{\mathbb{E}[\rho_\mathrm{p} e^{i\phi_\mathrm{p}} \rho_\mathrm{q} e^{-i\phi_\mathrm{q}}]}{\sqrt{\mathbb{E}[\rho_\mathrm{p}^2]\mathbb{E}[\rho_\mathrm{q}^2]}}$$

Since the second moment of Rayleigh distribution is the square of its parameter μ, the denominator can be deduced from the expression of μ computed in section 4.2 :

$$\sqrt{\mathbb{E}[\rho_\mathrm{p}^2]\mathbb{E}[\rho_\mathrm{q}^2]} = e^{\frac{\ln(10)}{20}(\mathrm{b_{dBp}} + \mathrm{b_{dBq}}) + (\frac{\ln(10)}{20}s_{\theta_s})^2(\mathrm{a_{dBp}}^2 + \mathrm{a_{dBq}}^2)}$$

The product of a pixel in the polarization channel p and its conjugate in the polarization channel q can be expressed using the scatterers parameters:

$$\rho_\mathrm{p} e^{i\phi_\mathrm{p}} \rho_\mathrm{q} e^{-i\phi_\mathrm{q}} = \frac{1}{N_s}\sum_{n=1}^{N_s} r_{\mathrm{p},n} e^{i\varphi_n} \sum_{n=1}^{N_s} r_{\mathrm{q},n} e^{-i\varphi_n}$$

$$= \frac{1}{N_s}\sum_{n=1}^{N_s} r_{\mathrm{p},n} r_{\mathrm{q},n} + \frac{1}{N_s}\sum_{n=1,m=1,n\neq m}^{n=N_s,m=N_s} r_{\mathrm{p},n} r_{\mathrm{q},m} e^{i(\varphi_n - \varphi_m)}$$

Since the phase difference $\varphi_n - \varphi_m$ is uniformly distributed on a 2π-interval :

$$\mathbb{E}[\frac{1}{N_s}\sum_{n=1,m=1,n\neq m}^{n=N_s,m=N_s} r_{\mathrm{p},n} r_{\mathrm{q},m} e^{i(\varphi_n - \varphi_m)}] = 0$$

while $\mathbb{E}[\frac{1}{N_s}\sum_{n=1}^{N_s} r_{\mathrm{p},n} r_{\mathrm{q},n}] = \frac{1}{N_s}\sum_{n=1}^{N_s}\mathbb{E}[e^{\frac{\ln(10)}{20}(\mathrm{b_{dBp}} + \mathrm{b_{dBq}}) + \frac{\ln(10)}{20}(\theta_{s\,n} - m_{\theta_s})(\mathrm{a_{dBp}} + \mathrm{a_{dBq}})}]$

Since the θ_{sn} are iid following a normal distribution of mean m_{θ_s} and standard deviation s_{θ_s}, the product $r_{\mathrm{p},n} r_{\mathrm{q},n}$ follows a log-normal distribution of parameters $\frac{\ln(10)}{20}(\mathrm{b_{dBp}} + \mathrm{b_{dBq}})$ and $\frac{\ln(10)}{20}s_{\theta_s}(\mathrm{a_{dBp}} + \mathrm{a_{dBq}})$. We thus have

$$\mathbb{E}[\rho_\mathrm{p} e^{i\phi_\mathrm{p}} \rho_\mathrm{q} e^{-i\phi_\mathrm{q}}] = e^{\frac{\ln(10)}{20}(\mathrm{b_{dBp}} + \mathrm{b_{dBq}}) + \frac{1}{2}(\frac{\ln(10)}{20}s_{\theta_s}(\mathrm{a_{dBp}} + \mathrm{a_{dBq}}))^2}$$

With these expressions, the theoretical expression of the degree of coherence is :

$$\gamma_{\mathrm{p,q}} = e^{-\frac{1}{2}(\frac{\ln(10)}{20}s_{\theta_s})^2(\mathrm{a_{dBp}} - \mathrm{a_{dBq}})^2}$$

which shows that, in order to get a degree of coherence lower to 1, which is observed in most of the natural scene, the distribution of the θ should have a variance, and the slope between the two input σ_0-curves should be different. These criteria are opposite to the ones developed in the section 4.2 There is thus a trade-off between the independence of the two polarimetric channels and the retrieval of the input σ_0-curve as an output of the simulation.

5 Results on textured terrains

5.1 Sensor, terrain and materials

5.1.1 Sensor and image parameters

The sensor has a TerraSAR-X configuration with a wavelength of 0.031m and an altitude of 514km, with a trajectory along the x-axis. The resolution is 1m in azimuth and 0.7m in slant range with an incidence angle θ of 40 degree. This allows us to get a mean 16 scatterers in each resolution cell for a flat terrain. With a zero-padding factor of 1.2 in azimuth and slant range, it reduces to 10 scatterers by resolution cells which as been shown to be enough to reproduce fully developed speckle [8]. Due to the layover, the number of scatterers can differ for the terrains used in the experiments.

5.1.2 Electromagnetic materials

The electromagnetic properties of each scatterers depends of the material in which their are made. In this experiment, two materials from [6] have been chosen : "Asphalt" in X-band and "Forage Crops" in L-band. These material have numerous measurement in the [0,90] interval. However, to get a value for every incidence angle, their values are linearly interpolated and extrapolated to cover the whole [0,90] interval. The resultant σ_0-curves are represented in figure 1.

Both materials correspond to a smooth surface with a specular return. The slopes of the σ_0-curve of the polarimetric channels are closer for the material "Forage crop", than for the material "Asphalt", where there is no measurement for $\theta < 10$ in the HV channels leading to a flat curve, and the slope of the HH channels is steeper than the in the two other channels for incidences over 30 degrees.

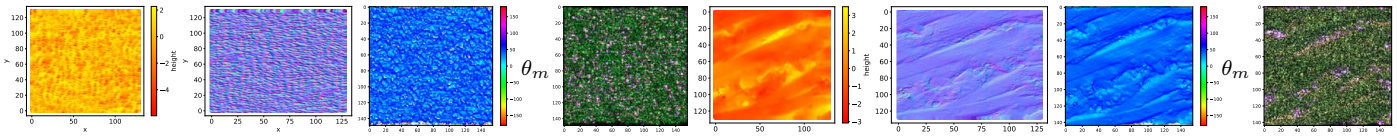

(a) (b) (c) (d) (e) (f) (g) (h)

Figure 3 Terrain Asphalt (a-b-c-d) and Tires on Snow (e-f-g-h) for $s = 1$m. (a-e) The height map in meter (b-f) the normal map in rgb with the red coding $n_x \in [-1, 1]$, the greed coding $n_y \in [-1, 1]$ and the blue coding $n_z \in [1, -1]$ (c-g) The pixel incidence angle θ_m for the a sensor incidence angle $\theta = 40°$ (d-h) SAR images in lexicographic basis with a threshold of $\mu_p + 3\sigma_p$ per channel (d) for the material "Asphalt" and (h) for the material "Forage Crop".

5.1.3 Terrains

The results are illustrated on two different terrains obtained from scanned materials : "Tires on snow" [11] and "Stone" [12]. The scanned terrain have a spacing of 0.25m for a dimension of 128m in both x and y, a zero-mean and height variance of $s = 0.1$ or $s = 1$. On figure 3, their height and normal are represented for $s = 1$. The normal is computed with a negative n_z. These dimensions are not realistic for this type of material but are representative of the degree of description of the terrain that we want to test.

The terrain "Tires on Snow" exhibits less variability than the terrain "Stone" for the same s, with higher pixels mean resultant length and a more concentrated histogram, as represented on Figure 4.

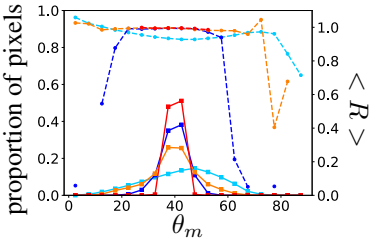

Figure 4 Distribution of the pixels' incidence angle and the pixels incidence angle concentration.
$-$ ■ $-$ histogram of the pixels incidence angle θ_m with 5° bins. - ● - mean of the pixels mean resultant length $< R >$ for each θ_m bin. Terrain "Tires on Snow" : ● $s = 1$m and ● $s = 0.1$m, and the terrain "Stone" ● $s = 1$m and ● $s = 0.1$m.

5.2 Modulus and ratio distribution

As opposed to random terrain, scanned materials allow to get texture in the output SAR images as illustrated in Figure 3 (d) and (h). Larger difference between HV and HH or VV can be observed when the pixel incidence angle is close to 0°.

To assess the difference between the input σ_0-curves and the output ones, the output Rayleigh distribution parameter is estimated using all the pixels having their incidence angle θ_m in a 5° bin. Figure 5 represents the input σ_0-curve, and the ouput σ_0-curve for 4 scenarii :

Fig. 5a Terrain "Stone", $s = 1$m, material "Asphalt".

Fig. 5b Terrain "Stone", $s = 0.1$m, material "Asphalt".

Fig. 5c Terrain "Tire on snow",$s = 1$m, material "Asphalt".

Fig. 5d Terrain "Stone", $s = 1$m, material "Forage crop".

These figures show that the output σ_0-curves are higher than the input ones only for the terrain "Stone" with $s = 1$m for both materials, when $\theta > 10°$ for the channels HH and VV and when $\theta > 50°$ for the channels HV. As shown in Figure 4, the terrain "Stone" with $s = 1$m is the terrain that exhibits the more variations in incidence angle.

The output ratios HV/HH and VV/HH are below the input ones only for the Terrain "Stone" with $s = 1$m, and the material "Asphalt". This can be explain by the fact that the terrain "Tire on snow" and the terrain "Stone" $s = 0.1$m have a smaller incidence angle variability and that the slope of σ_0-curves are similar in the different polarimetric channels for the material "Forage Crop".

To compare these output σ_0-curves and ratio to the one predicted by the random terrain experiment presented in section 4, we deduced the standard deviation of the incidence angle distribution from the pixels' mean resultant length using the following formula : $s_{\theta_s} = \frac{180}{\pi}\sqrt{-2\ln(R)}$ (in degrees) as if the incidence angle distributions were following a wrapped normal distribution. The results are represented by the squares on Figure 5. If the output σ_0-curves and ratio have the same order of magnitude than the one predicted by the random terrain experiment, their values do not match. This can be explain by a θ_s distribution different from the wrapped normal distribution (when $R = 0.92$, $s_{\theta_s} = 0.23$, which would lead to truncated value). Furthermore, for $\theta < 10°$, the discrepancy between the outputσ_0-curves and the values predicted by the random terrain experiment could be resulting of a non-symetrical incidence angle distribution, since angles cannot be smaller than 0°. A better measure of the scatterers incidence angle distribution should be performed in order to have a predictive model.

5.3 Degree of coherence

In our experiment, the degree of coherence, estimated using a boxcar filter of 5 pixels by 5 pixels, showed very small variability given the incidence angle. The mean degree of coherence estimated over the full image is summarized in table 1 in the eight configurations presented in this article. As expected from the random terrain experiment, the degree of coherence $\gamma_{p,q}$ departs from one when the terrain exhibit a larger variability and the slopes of the σ_0-curve in the two polarimetric channels differ. Thus, $\gamma_{p,q}$ is smaller for s=1m than for s=0.1, for the Terrain "Stone" than the Terrain "Tire on Snow", for the material "Asphalt" than for the material "Forage crop", and for the polariza-

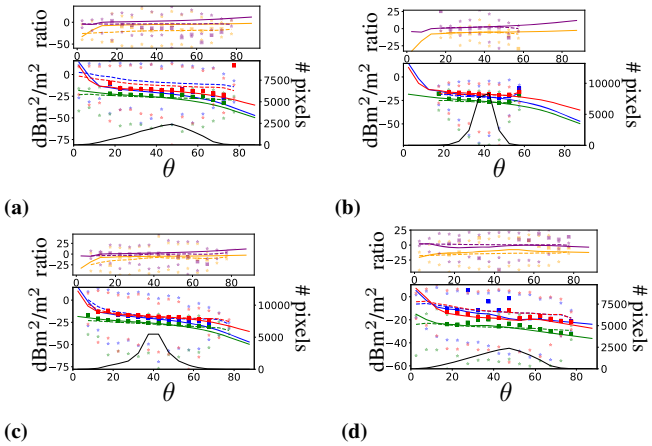

Figure 5 Input and output σ_0-curve and ratio between the σ_0-curve in the case of (a) Terrain "Stone", $s = 1$m, material "Asphalt" (b) Terrain "Stone", $s = 0.1$m, material "Asphalt (c) Terrain "Tire on snow", $s = 1$m, material "Asphalt (d) Terrain "Stone", $s = 1$m, material "Forage crop". For each sub-figures, on the bottom figure is represented the σ_0-curve : σ_{0HH} $\tilde{\mu}_{HH}$ σ_{0HV} $\tilde{\mu}_{HV}$ σ_{0VV} $\tilde{\mu}_{VV}$ and on the top figure is represented the ratio curve : $\frac{\sigma_{0HV}}{\sigma_{0HH}}$ $\frac{\tilde{\mu}_{HV}}{\tilde{\mu}_{HH}}$ $\frac{\sigma_{0VV}}{\sigma_{0HH}}$ $\frac{\tilde{\mu}_{VV}}{\tilde{\mu}_{HH}}$ The stars represent the maximum and the minimum values for each bin. The squares represent the value expected if the terrain where following the random models.

tion HH and HV than for the polarization HH and VV. The lower degree of coherence is thus $\gamma_{HH,HV} = 0.52$ for he Terrain "Stone" with s=1m and the material "Asphalt".

Terrain	Stone				Tires on Snow			
Material	Forage Crop		Asphalt		Forage Crop		Asphalt	
s (m)	0.1	1	0.1	1	0.1	1	0.1	1
$\gamma_{HH,HV}$	0.99	0.92	1.00	0.52	1.00	0.98	1.00	0.85
$\gamma_{HH,VV}$	0.99	0.96	1.00	0.94	1.00	0.98	1.00	0.96

Table 1 Mean degree of coherence between the polarimetric channels in the eights configurations studied in this article.

6 Conclusion

In this article we studied the distribution of the modulus and the degree of coherence of a SAR images simulated by the coherent sum of a finite number of scatterers. Their backscattered energy is computed from σ_0-curve and parameterized by their incidence angle only θ_s. The position of the scatterers and thus their incidence angle θ_s depends of the terrain's roughness, that correspond to the standard deviation of the incidence angle s_{θ_s} in the case of random terrain or the rms of the height s for scanned materials. The scatterers phase depends only from their distance to the sensor and is the same the different polarimetric channels.

The study of the difference between the input and the output σ_0-curve on random and scanned terrains shows that it increases with the variance of the local incidence angle distribution and the square of the slope of the input σ_0-curve. Thus, the ratio between two polarizations can be retrieved if the two σ_0-curves slope have the same square. In these experiments, the output σ_0-curve on scanned material could not be predicted from the results on random terrain, very likely due to the lack of precision in the measurement of the variability of the local incidence angle.

The degree of coherence depends on the variance of the local incidence angle distribution and square of the slopes difference. Even with the same phase in the different polarimetric channels, a decoherence can be observed. However, in order to retrieve the degree of coherence observed in real images, a phase difference between the polarimetric channels should be added.

7 Literature

[1] Shane R. Cloude and Eric Pottier. An Entropy Based Classification Scheme for Land Applications of Polarimetric SAR. *IEEE Transactions on Geoscience and Remote Sensing*, 35(1):68–78, 1997.

[2] Yisok Oh, Kamal Sarabandi, and Fawwy Ulaby. An Empirical Model and an Inversion Technique for Radar Scattering from Bare Soil Surfaces. *IEEE Geoscience and Remote Sensing Magazine*, 30(2):370–381, 1993.

[3] Jiancheng Shi, James Wang, Ann Y. Hsu, Peggy E. O'Neill, and Edwin T. Engman. Estimation of bare surface soil moisture and surface roughness parameter using L-band SAR image data. *IEEE Transactions on Geoscience and Remote Sensing*, 35(5):1254–1266, 1997.

[4] Francesco Mattia, Thuy Le Toan, Jean-Claude Souyris, Giacomo De Carolis, Nicolas Floury, Franco Posa, and Guido Pasquariello. The effect of surface roughness on multifrequency polarimetric sar data. *IEEE Transactions on Geoscience and Remote Sensing*, 35(4):954–966, 1997.

[5] D Schuler, J Lee, D Lasilingam, and G Nesti. Surface roughness and slope measurements using polarimetric SAR data - Geoscience and Remote Sensing, IEEE Transactions on . *IEEE Transactions on Geoscience and Remote Sensing*, 40(3):687–699, 2001.

[6] Fawwaz T Ulaby and M. Graig Dobson. *Handbook of Radar Scattering: Statistics for Terrain*. 1989.

[7] Joseph W. Goodman. *Statistical Optics*. Wiley, 2000.

[8] Flora Weissgerber and Nicolas Trouvé. Simulation of clutter based on a sum of scatterers. In *International Radar Conference*, volume 1, pages 0–5, 2019.

[9] Joseph W Goodman. Speckle with a finite number of steps. *Applied optic*, 47(4):111–118, 2008.

[10] Kanti V. Mardia and Peter E. Jupp. *Directional Statistics*. Wiley, 1999.

[11] https://www.textures.com/download/3dscans0452/133749.

[12] https://www.textures.com/download/3dscans0526/134351.